
A neural surrogate solver for radiation transfer

Anonymous Author(s)

Affiliation
Address
email

Abstract

Radiative transfer is often the dominant mode of heat transfer in fires, and solving the governing radiative transfer equation (RTE) in CFD fire simulations is computationally intensive. This work develops a versatile toolkit for training neural surrogates to solve various RTEs across different geometries and boundary conditions. Principal Component Analysis is applied for dimension reduction to enable efficient training of high-dimensional surrogate solvers. The mesh free nature of these surrogates enables them to overcome the ray effect suffered by traditional solvers. Our results demonstrate that neural surrogate can provide fast and accurate radiation predictions for practical problems important to fire safety research.

1 Introduction

FireFOAM Wang et al. [2011, 2014] is an open-source CFD solver for large-scale fires, capable of modeling all of the complex physics that occur during an industrial fire, including heat transfer, pyrolysis, turbulent combustion, and water suppression. Despite being highly scalable on parallel computers, the solver takes several days to over two months to simulate practical fires. The high computational cost is primarily attributed to solving pressure and radiation equations.

GPU acceleration in FireFOAM is achieved by employing NVIDIA’s AMGx solvers to offload linear solver computations from CPUs to GPUs, significantly reducing the time required to solve the pressure equation `p_rghEqn`. However, since matrix and vector assembly still occur on CPUs, this method is not applicable for radiation calculations using the discrete ordinate method, which would require extensive code refactoring to be effective on GPUs.

The recent advances in machine learning has transformed the way we approach scientific computing. Mishra and Molinaro Mishra and Molinaro [2021] demonstrated that physics-informed neural networks (PINNs) can effectively solve the radiative transfer equation (RTE) with fixed temperature and absorption coefficients, noting their ease of implementation, speed, robustness, and accuracy. Recent research Lu and Wang [2024] has expanded this approach by using physics-informed deep operator networks (PI-DeepONets) to solve parameterized RTEs, achieving significant speedups for 1D radiation problems.

The present study extends the work of Lu and Wang [2024] by developing surrogate RTE solvers for multi-dimensional radiation problems. We introduce a new model formulation that solves RTEs with complex boundary conditions. A novel application of Principal Component Analysis (PCA) encodes input functions into low-dimensional representations, resulting in more compact DeepONet architectures. The new methodology is implemented in a flexible and extensible sciML toolkit for

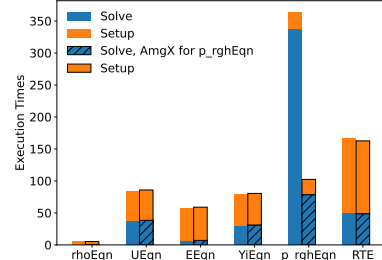


Figure 1: Comparison of times spent in solving different PDEs in FireFOAM.

38 training neural surrogate RTE solvers using physics-informed, data-driven, or hybrid loss functions.
 39 We utilize the developed library to solve radiation problems in fire safety research.

40 2 Methods

41 In CFD simulations, radiation is incorporated into the energy equation as a volumetric radiative
 42 heat loss term. This requires solving the radiative intensity field $I(\mathbf{x}, \mathbf{s})$ at various locations \mathbf{x} and
 43 directions \mathbf{s} from the radiative transport equation (RTE), given by

$$44 \quad \mathbf{s} \cdot \nabla I(\mathbf{x}, \mathbf{s}) = -\kappa(\mathbf{x})I(\mathbf{x}, \mathbf{s}) + \kappa(\mathbf{x})I_b(\mathbf{x}), \quad (1)$$

45 subject to the boundary condition imposed for radiation rays emitting from bounding surfaces to the
 radiatively participating media within the domain

$$46 \quad I(\mathbf{x}, \mathbf{s}) = \epsilon(\mathbf{x})I_b(\mathbf{x}) + \frac{\rho^d(\mathbf{x})}{\pi} \int I(\mathbf{x}, \mathbf{s}')|\mathbf{n}(\mathbf{x}) \cdot \mathbf{s}'|d\Omega(\mathbf{x}) + \rho^s(\mathbf{x})I(\mathbf{x}, \mathbf{s}_s(\mathbf{x}, \mathbf{s})). \quad (2)$$

46 \mathbf{n} denotes the boundary surface normal, $\mathbf{s}_s = \mathbf{s} - 2\mathbf{n}(\mathbf{n} \cdot \mathbf{s})$ is the direction of a specular reflection,
 47 and $d\Omega$ is the solid angle.

48 The input functions of the RTE are the absorption coefficient $u_1 (= -\kappa) \in \mathcal{U}_1$, the black body
 49 emissive power $u_2 (= I_b) \in \mathcal{U}_2$, the surface emissivity $u_3 (= \epsilon) \in \mathcal{U}_3$, the diffusive reflection
 50 coefficient $u_4 (= \rho^d) \in \mathcal{U}_4$, and the specular reflection coefficient $u_5 (= \rho^s) \in \mathcal{U}_5$. Boundary
 51 operators are generalized and parameterized, whereas prior work Lu and Wang [2024] assumed
 52 black walls at fixed temperatures. We use a DeepONet to approximate the RTE solution operator
 53 $G : \mathcal{U}_1 \times \mathcal{U}_2 \times \mathcal{U}_3 \times \mathcal{U}_4 \times \mathcal{U}_5 \rightarrow \mathcal{I}$ which maps input functions to the solution $I(\mathbf{x}, \mathbf{s}) \in \mathcal{I}$ as

$$46 \quad G(u_1, \dots, u_5) = I. \quad (3)$$

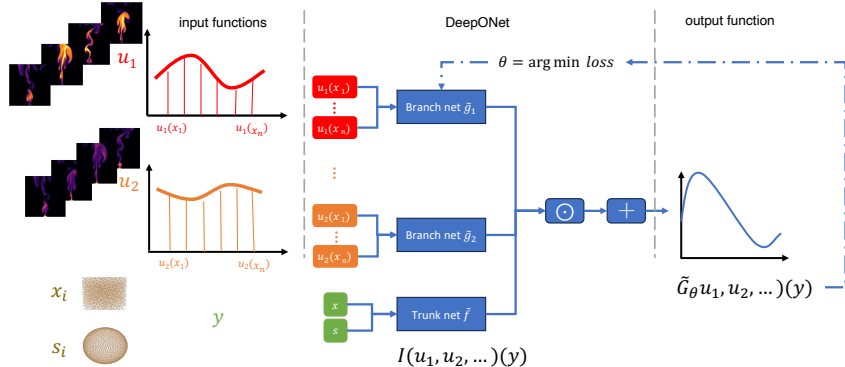


Figure 2: The architecture of DeepONet for learning the mapping between function spaces. We only show two of the five random coefficients for simplicity.

DeepONet comprises two main components: the branch net and the trunk net (see Lu et al. [2021]), as illustrated in Figure 2. As shown in the leftmost panel, the branch nets g_1, \dots, g_5 encode input functions $\mathbf{u}_1(\mathbf{x}), \dots, \mathbf{u}_5(\mathbf{x})$ at a fixed number of discrete sensor locations $x_i, i = 1, \dots, n$. The trunk net f encodes the location and direction $\mathbf{y} = (\mathbf{x}, \mathbf{s})$ where the output function $G(\mathbf{u}_1, \dots, \mathbf{u}_5)(\mathbf{y})$ is evaluated within a given domain. The multiple-input DeepONet prediction is

$$\tilde{G}_{\Theta}(\mathbf{u}^1, \dots, \mathbf{u}^5)(\mathbf{y}) = \mathcal{F}_{\Theta_0}(\mathbf{y}) \odot \mathcal{G}_{\Theta_1}(\mathbf{u}^1) \odot \dots \odot \mathcal{G}_{\Theta_5}(\mathbf{u}^5) + b$$

54 where \odot is the Hadamard product of the H outputs from each MLP, b is a trainable bias parameter,
 55 and $\Theta = \cup_{i=0}^R \Theta_i$ aggregates all networks parameters.

56 The data for training a DeepONet is the Cartesian product of random coefficients $(\mathbf{u}_k^1, \dots, \mathbf{u}_k^5)_{k=1}^{N_{RC}}$
 57 and collocation points $(\mathbf{x}_i, \mathbf{s}_i)_{i=1}^{N_C}$. The collocation points are input to the trunk net while the random
 58 coefficients are sampled at *sensor locations* to get *sensor values* which are input to the branch nets.
 59 Our implementation support both aligned datasets, where the sensor locations match the collocation
 60 points, and unaligned datasets. Moreover, we lazily constructs batches of the Cartesian product
 61 dataset on GPU to significantly reduce the time spent loading data.

We support Principal Component Analysis (PCA) to reduce the number of sensor values. Auto-encoders for SciML have also shown success for dimensionality reduction Kontolati et al. [2023], but they require additional training for the encoder and are not amenable to distributed evaluation. PCA instead can be done via a simple matrix vector multiplication in a distributed manner when integrated in parallel CFD solvers.

The weighted hybrid loss function combines terms for the RTE (1), boundary condition (2), and data from a traditional solver into

$$\mathcal{L}(\Theta) = \omega_{\text{RTE}} \|\mathcal{R}_{\text{RTE}}(\tilde{G}_\Theta, \mathcal{D}_{\text{RTE}})\| + \omega_{\text{BC}} \|\mathcal{R}_{\text{BC}}(\tilde{G}_\Theta, \mathcal{D}_{\text{BC}})\| + \omega_{\text{data}} \|\mathcal{R}_{\text{data}}(\tilde{G}_\Theta, \mathcal{D}_{\text{data}})\|.$$

Here ω are the weights, \mathcal{R} are the residuals, and \mathcal{D} are subsets of the sensor-collocation data with $\mathcal{D}_{\text{data}}$ also containing solution data from the reference solver. The gradient in (1) is evaluated exactly using automatic differentiation, while the integral in (2) is approximated using either Gauss-Legendre quadrature or Quasi-Monte Carlo Niederreiter [1992]. These cubature routines are also used to infer the incident radiation, radiative heat flux, or radiative heat loss.

The core functionalities of the developed sciML library are implemented into two abstract classes. The first constructs the sensor-collocation datasets \mathcal{D} while the second defines the loss function $\mathcal{L}(\Theta)$ by implementing both the residuals \mathcal{R} and the DeepONet \tilde{G}_Θ . The complete code will be made available upon publications.

3 Numerical Experiments

Numerical experiments are conducted using the developed sciML library, showcasing trained neural surrogates solving RTEs with complex boundary conditions and in practical settings of fire radiation transfer. The selected test problems include a cylinder enclosure problem from [Chui et al., 1992, Fig. 5], the four special cases considered in [Ge et al., 2016, Section 4.3], and the small pool fire case from FireFOAM/tutorials.

DeepONet training hyperparameters are summarized below where L_T and L_B are the number of hidden layers in trunk and branch nets respectively, γ is the learning rate, B is the the equal batch size across datasets, and E is the number of epochs. Note that the number of network parameters $|\Theta|$ is also a function of the number of sensor locations which is described in the following paragraphs. All training uses the AMSGrad variant of the Adam optimizer.

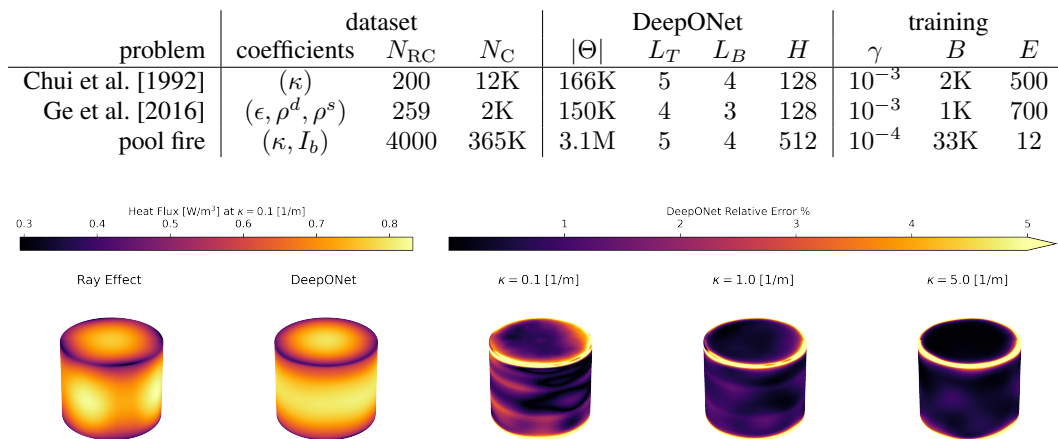


Figure 3: DeepONets overcome the ray effect and yield small pointwise relative errors.

A first test solves gas radiation transfer in a cylindrical enclosure. Boundaries are cold black walls and gas temperature is constant. The DeepONet was trained with $N_{\text{RC}} = 200$ random realizations of constant κ between $\kappa = 0.01 [\text{m}^{-1}]$ and $\kappa = 6 [\text{m}^{-1}]$ and no traditional solver data was provided i.e. this was a purely physics-informed training. L_2 relative errors of 1.53%, 1.17%, and 1.88% were attained for $\kappa = 0.1$, $\kappa = 1$, and $\kappa = 5$ respectively with the pointwise relative errors also shown in Figure 3. The discrete ordinate method in FireFOAM, when the angular discretization is coarse, suffers from the ray effect, which is quickly mitigated in DeepONet.

96 A second test problem in [Ge
 97 et al., 2016, Section 4.3] con-
 98 siders gas radiation transfer in a
 99 rectangular domain with mixed
 100 boundary conditions. The gas
 101 temperature is prescribed and the
 102 absorption coefficient is constant
 103 $\kappa = 0.5 \text{ [m}^{-1}\text{]}$, while ϵ, ρ^d, ρ^s
 104 are unknown piecewise constant
 105 functions satisfying $\epsilon + \rho^d + \rho^s =$
 106 1. The top and bottom bound-
 107 ary have fixed $\epsilon = 1$ while the
 108 left and right boundary are ran-
 109 dom constants $\epsilon_{LR}, \rho_{LR}^d$, and
 110 ρ_{LR}^s . The DeepONet is trained
 111 on $N_{RC} = 259$ random realiza-
 112 tions of $\epsilon_{LR}, \rho_{LR}^d$, and ρ_{LR}^s , and
 113 tested with the parameters spec-
 114 ified in [Ge et al., 2016, Section
 115 4.3]. Figure 4 compares the predicted
 116 volumetric heat loss along a vertical slice of the domain
 between DeepONet and the P_7 model from Ge et al. [2016].

117 The third problem trains DeepONet on $N_{RC} = 4\text{K}$ FireFOAM pool fire simulation snapshots, which
 118 use 151×151 cells and 16 discrete ordinates. The high-dimensional datasets are encoded into
 119 lower-dimensional latent spaces using PCA, reducing the branch net input size from 23K to 500.
 120 Figure 5 compares predicted incident radiation results on withheld testing realizations. Notably, the
 121 DeepONet approximation does not suffer from the ray effect observed in the discrete ordinate solver.

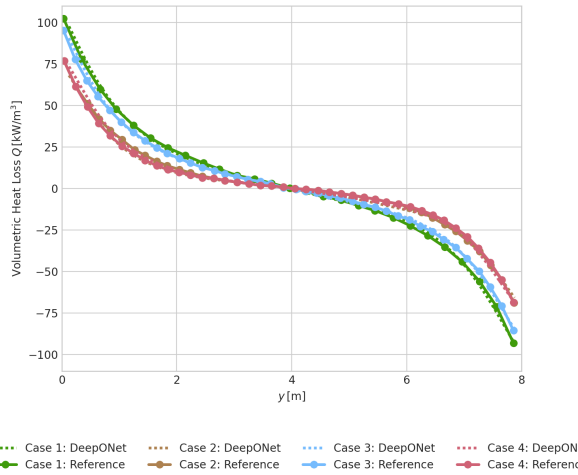


Figure 4: Comparison of DeepONet predicted heat loss with the P_7 models of Ge et al. [2016].

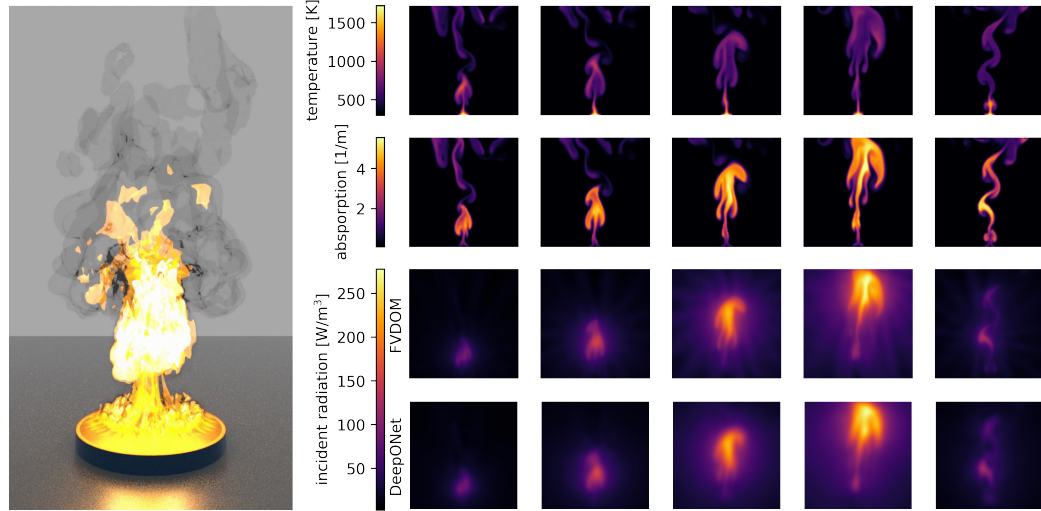


Figure 5: Comparison of predicted incident radiation in a pool fire between DeepONet and discrete-ordinate solvers.

122 4 Conclusions

123 This work introduces a new ML toolkit for training neural surrogates to solve radiation transfer.
 124 Users can select from 1, 2, or 3D geometries and random coefficients from the governing equation or
 125 boundary condition. Principal Component Analysis (PCA) can be optionally used to reduce the branch
 126 network input sizes for more compact DeepONet architectures. The SciML models are trained using
 127 physics-informed, data-driven, or hybrid loss functions. While this article only describes DeepONets,
 128 the implementation also supports PINNs. The next step will focus on evaluating performance and
 129 deploying neural surrogate solvers in CFD of large-scale fires.

130 **References**

- 131 EH Chui, GD Raithby, and PMJ Hughes. Prediction of radiative transfer in cylindrical enclosures
132 with the finite volume method. *Journal of Thermophysics and Heat transfer*, 6(4):605–611, 1992.
- 133 Wenjun Ge, Michael F Modest, and Somesh P Roy. Development of high-order pn models for
134 radiative heat transfer in special geometries and boundary conditions. *Journal of Quantitative
135 Spectroscopy and Radiative Transfer*, 172:98–109, 2016.
- 136 Katiana Kontolati, Somdatta Goswami, George Em Karniadakis, and Michael D Shields. Learn-
137 ing in latent spaces improves the predictive accuracy of deep neural operators. *arXiv preprint
138 arXiv:2304.07599*, 2023.
- 139 Lu Lu, Pengzhan Jin, Guofei Pang, Zhongqiang Zhang, and George Em Karniadakis. Learning
140 nonlinear operators via deeponet based on the universal approximation theorem of operators. *Nat.
141 Mach. Intell.*, 3(3):218–229, 2021.
- 142 Xiaoyi Lu and Yi Wang. Surrogate modeling for radiative heat transfer using physics-informed deep
143 neural operator networks. *Proceedings of the Combustion Institute*, 40(1-4):105282, 2024.
- 144 Siddhartha Mishra and Roberto Molinaro. Physics informed neural networks for simulating radiative
145 transfer. *J Quant Spectrosc Radiat Transf.*, 270:107705, 2021.
- 146 Harald Niederreiter. *Random number generation and quasi-Monte Carlo methods*. SIAM, 1992.
- 147 Yi Wang, Prateep Chatterjee, and John L de Ris. Large eddy simulation of fire plumes. *Proceedings
148 of the Combustion Institute*, 33(2):2473–2480, 2011.
- 149 Yi Wang, Karl V Meredith, Xiangyang Zhou, Prateep Chatterjee, Yibing Xin, Marcos Chaos, Ning
150 Ren, and Sergey B Dorofeev. Numerical simulation of sprinkler suppression of rack storage fires.
151 *Fire Safety Science*, 11:1170–1183, 2014.